*D. F. Lefebvre**

Hydrostatic Pressure Effect on Life Prediction in Biaxial Low-Cycle Fatigue

REFERENCE Lefebvre, D. F., **Hydrostatic pressure effect on life prediction in biaxial low-cycle fatigue**, *Biaxial and Multiaxial Fatigue*, EGF 3 (Edited by M. W. Brown and K. J. Miller), 1989, Mechanical Engineering Publications, London, pp. 511–533.

ABSTRACT The biaxial low-cycle fatigue of A-516 Grade 70 steel is evaluated by means of experimental data from 44 fully-reversed strain-controlled tests on thin-walled tubes subjected to combinations of cyclic axial loading and external–internal pressure. Fatigue results are presented, including the determination of the principal stresses, the axial and circumferential elastic moduli, the effective Poisson ratio, and the elastic, plastic, and total components of the three principal strains. Stress and strain-based criteria, taking into account the hydrostatic pressure effect on the fatigue life, are proposed. In terms of stresses, a relation of the form $G(I_1, I_2, N_f) = 1$ is suggested, while in terms of strains, the best correlation is obtained with the relation $\frac{1}{2}\gamma_{max} + f(\varepsilon_s) = C$, where $\varepsilon_s = \varepsilon_n$ (the normal strain acting on the maximum shear strain plane) when stress ratios are negative, or $\varepsilon_s = \varepsilon_m$ (the hydrostatic tensile strain) when stress ratios are positive.

Introduction

Most metallic structures and components are subject to complex cyclic load histories which cause metallurgical damage in highly stressed locations that eventually may result in fatigue failure. In the study of multiaxial low-cycle fatigue, engineers attempt to derive, from simple laboratory test data, theories which will permit an adequate assessment of fatigue behaviour of material under complex stress–strain conditions. Many studies have been made both to generate valid experimental data and to propose adequate criteria for correlating the available test results. Most experimental results have been obtained from cyclic tension–torsion tests on thin-walled tubes for which the strain ratios are limited between -1 and $-\nu$. However, there exist very few experimental data for the positive strain ratios, since they require complicated testing devices using cruciform specimens or thin-walled tubes subjected to combinations of axial load and pressure. This investigation was undertaken to assist the development of fatigue life prediction methods for components under general states of large cyclic strains.

In this study, the high-strain biaxial fatigue behaviour of A-516 Grade 70 steel is experimentally examined. The experiments have been conducted under biaxial states of controlled strain. The specimens used were thin-walled tubes subjected to combinations of cyclic axial load and fluctuating internal–external pressure. Fatigue results from 44 tests are presented, including the determi-

* Department of Civil Engineering, Université de Sherbrooke, Quebec, Canada J1K 2R1.

nation of the principal stresses, the axial and circumferential elastic moduli, the effective Poisson ratio, and the elastic, plastic, and total components of the three principal strains. Fatigue life prediction is evaluated by means of a stress-based and a strain-based criterion, taking into account the hydrostatic stress (or the hydrostatic strain) effect on the fatigue life.

Notation

A_o	Initial cross-sectional area
b, c	Strength and ductility fatigue exponents
d_e, d_i, d_m	External, internal, and mean diameters
E	Young's modulus
E^e	Biaxial elastic modulus
F^{max}, F^{min}	Maximum, minimum axial load
I_1	First stress invariant, $I_1 = \sigma_{kk}$
I_2	Second stress invariant, $I_2 = \frac{1}{2}(\sigma_{kk}^2 - \sigma_{ij}\sigma_{ij})$
J_2	Second deviatoric stress invariant, $J_2 = (I_1^2/3) - I_2$
N_f	Number of cycles to failure
P_e	Constant external pressure
P_i^{max}, P_i^{min}	Maximum, minimum internal pressure
t	Initial wall thickness
TF	Triaxiality factor, $TF = I_1/(3J_2)^{1/2}$
γ_F	Failure strain for cyclic torsion
$\frac{1}{2}\gamma_{max}$	Maximum shear strain
γ_S	Fatigue biaxial strain parameter
$\bar{\varepsilon}$	Equivalent strain
ε_f'	Fatigue ductility coefficient
ε_F	Failure strain for cyclic axial loading
ε_m	Hydrostatic tensile strain (three times); $\varepsilon_m = \varepsilon_1 + \varepsilon_2 + \varepsilon_3$
ε_n	Normal strain on the plane of maximum shear strain
$\varepsilon_1 > \varepsilon_2 > \varepsilon_3$	Principal strains
ν	Poisson's ratio
ν_{eff}	Effective Poisson ratio
ϱ	Strain ratio; $\varrho = \varepsilon_t/\varepsilon_a$
$\bar{\sigma}$	Equivalent stress
σ_f'	Fatigue strength coefficient
σ_F	Failure stress for cyclic axial loading
σ_n	Normal stress on the plane of maximum shear stress
σ_S	Fatigue biaxial stress parameter
$\sigma_{0.2\%}$	Yield stress at 0.2%
$\sigma_1 > \sigma_2 > \sigma_3$	Principal stresses
τ_{max}	Maximum shear stress

Indices

a, t, r	Axial, circumferential, and radial directions
e, p	Elastic and plastic components

Previous work on multiaxial low-cycle fatigue

Experimental and theoretical work on multiaxial low-cycle fatigue was recently reviewed by Krempl (**1**), Brown and Miller (**2**), and Garud (**3**). A brief review is now presented in which fatigue life prediction is evaluated by means of stress-based, strain-based, and energy-based criteria.

Stress-based criteria, adapted from static yield criteria, were applicable primarily in the high-cycle fatigue regime. Two criteria, namely the Tresca criterion and the von Mises criterion, have sometimes been used successfully in the low-cycle fatigue life prediction of ductile metals. Other stress-based criteria have been developed later, from a wide variety of results on various steels and aluminium alloys. For isotropic materials, they can be expressed in two general forms. The first one is defined in terms of the stress invariants by (**1**)(**4**)

$$G(I_1, I_2, N_F) = 1 \tag{1}$$

A particular form of this equation is the Gough ellipse quadrant relation expressed as follows

$$\left(\frac{\sigma}{\sigma_F}\right)^2 + \left(\frac{\tau}{\tau_F}\right)^2 = 1 \quad \text{or} \quad \frac{I_1^2}{\sigma_F^2} - \frac{I_2}{\tau_F^2} = 1 \tag{2}$$

in which σ_F and τ_F represent the stresses for failure at a given number of cycles for axial and shear cycling alone. Gough's relation reduces to the Tresca criterion when $\sigma_F/\tau_F = 2$, and to the von Mises criterion when $\sigma_F/\tau_F = \sqrt{3}$. Sines (**5**) has proposed a relation which takes into account the static stresses superimposed on the cyclic stresses

$$aJ_{2\,\text{cycl.}}^{1/2} + bI_{1\,\text{stat.}} = 1 \tag{3}$$

The second form of the stress-based failure criteria is

$$\tau_{max} + f(\sigma_n) = 1 \tag{4}$$

According to this theory, failure occurs at a given number of cycles when the maximum shear stress, modified by the normal stress acting on the plane of maximum shear stress, reaches the failure stress in pure shear. Particular expressions of equation (4) have been proposed by Stanfield (**3**)

$$\tau_{max} + k_1\sigma_n = \tau_F \quad \text{with} \quad k_1 = \frac{\tau_F - \sigma_F/2}{\sigma_F/2} \tag{5}$$

and McDiarmid (**6**)

$$\tau_{max} + k_2\sigma_n^{1.5} = \tau_F \quad \text{with} \quad k_2 = \frac{\tau_F - \sigma_F/2}{(\sigma_F/2)^{1.5}} \tag{6}$$

These criteria reflect the physical observation that low-cycle fatigue depends on superimposed pressure. They have been experimentally verified for ductile metals under cyclic tension–torsion loadings (**2**)(**7**)–(**9**) and under fluctuating internal pressure and axial load (**6**).

In early studies, the strain-based criteria were also direct adaptations of static failure criteria. The octahedral shear strain criterion has been widely used in tension–torsion low-cycle fatigue, successfully in some cases, but not in others (**2**). An effective total octahedral shear strain criterion has been proposed by Schewchuck *et al.* (**10**) in which an effective Poisson ratio, varying from its elastic value to its plastic value, is used to determine the third principal strain. This approach has been verified by Ellison *et al.* (**11**) from experimental results on RR58 aluminium alloy. However, serious fundamental objections were raised against the criteria extended from yield theories. It has been demonstrated (**12**)(**13**) that superposed hydrostatic pressure influences the fatigue life in the low-cycle region. The most dangerous state of strain is equibiaxial loading where, in addition to an equivalent strain, there is also a tensile strain across the crack plane. Libertiny (**12**) and Pascoe *et al.* (**13**) have proposed a modification of the Coffin–Manson equation

$$\Delta\varepsilon_{eq.} N_f^{\alpha} = C \quad \text{with} \qquad C = g(C_u, M), \quad \alpha = h(\alpha_u, M) \tag{7}$$

where C and α are material constants, C_u and α_u are the values of C and α for the uniaxial case, and M is a stress- or strain-dependent parameter. Different expressions for the equivalent strain amplitude and the parameter M have been chosen according to the experimental data. Such theories are no longer widely used, since they require extensive experimental studies for the determination of the empirical parameters.

Another approach to the biaxial low-cycle problem, based on a physical interpretation of mechanisms of fatigue crack growth, was developed by Brown and Miller (**14**). According to this theory, failure under multiaxial fatigue is governed by the maximum shear strain modified by the normal strain on maximum shear strain planes. This theory, represented graphically by contours of equal life on a 'Γ-plot', is expressed mathematically by

$$(\varepsilon_1 - \varepsilon_3)/2 = f\{(\varepsilon_1 + \varepsilon_3)/2\} \tag{8}$$

In their analysis, the authors differentiate between two types of cracks: in case A, corresponding to a strain ratio between -1 and $-\nu$, cracks propagate along the surface of the specimen, while in case B, corresponding to a strain ratio between $-\nu$ and 1, cracks propagate away from the surface. From a wide range of experimental data, they proposed the specific forms for equation (8) (**15**)

$$\begin{aligned} \left(\frac{\gamma_{max}}{2g}\right)^j + \left(\frac{\varepsilon_n}{h}\right)^j &= 1 \qquad \text{for case A} \\ \gamma_{max}/2 &= C \qquad \text{for case B} \end{aligned} \tag{9}$$

However, they state that the function, f, may vary with life and material properties and that the shape of the Γ-plot depends on Poisson's ratio. Blass and Zamrik (**2**)(**16**) indicate, from cyclic tension–torsion tests on 304 stainless steel, that a failure criterion based on the shear and normal strains on the plane of maximum shear strain would be more effective than those based on

equivalent strain. They use the least square method to fit all the data and suggest different forms for equation (8) according to the type of cracks. The principal objection against Brown and Miller's theory is that it cannot explain the life reduction experimentally observed for the equibiaxial state of strain (12)(13).

The hydrostatic stress effect on the fatigue life has also been analyzed by means of the concept of effective ductility in multiaxial loading. Davis and Connelly (17) have primarily demonstrated that loss of ductility always accompanies triaxial tension. They have obtained the effective ductility by dividing the tensile ductility by a triaxiality factor

$$TF = \frac{\sqrt{2}(\sigma_1 + \sigma_2 + \sigma_3)}{\{(\sigma_1 - \sigma_2)^2 + (\sigma_2 - \sigma_3)^2 + (\sigma_3 - \sigma_1)^2\}^{1/2}} \tag{10}$$

TF is equal to zero for pure torsion, to one for uniaxial loading, and to two in the equibiaxial case. This concept has recently been used in the development of low-cycle fatigue life equations (18)–(20).

The modified equivalent plastic strain is expressed as follows

$$\Delta\bar{\varepsilon}^{*\mathrm{P}} = MF \cdot \Delta\bar{\varepsilon}^{\mathrm{P}} \tag{11}$$

where $\Delta\bar{\varepsilon}^{\mathrm{P}}$ is the equivalent plastic strain range, $MF = 1/(2 - TF)$ if $TF \leqslant 1$ and $MF = TF$ if $TF \geqslant 1$, according to Manson *et al.* (18), $MF = 2^{(TF-1)}$, according to Marloff *et al.* (19), and $MF = 1/(1 - mTF)$ with $0 \leqslant m \leqslant 0.5$, according to Mowbray (20). Unfortunately, data in low-cycle fatigue, for which elastic and plastic strain components can be separated are very limited and the correlation of some available data by means of equation (11) does not lead to a good agreement.

Attempts have been made to relate fatigue life with the plastic strain energy dissipated during a cycle. This approach is based on the hypothesis that fatigue damage is proportional to the change in internal strain energy. In uniaxial low-cycle fatigue, it has been demonstrated (21)–(23) that fatigue life can be correlated with the plastic strain energy per cycle W_c by the following relation

$$W_c = \frac{1 - n'}{1 + n'} \Delta\sigma \cdot \Delta\varepsilon^{\mathrm{P}} = KN_f^{\alpha} \tag{12}$$

where n' is the cyclic hardening exponent. Generalization of this relation to the multiaxial case has been proposed by Ellyin (24) and Leis (25). They proposed a total octahedral internal energy parameter per cycle

$$U_T = \bar{\sigma}_m \Delta\bar{\varepsilon} + \Delta\bar{\sigma} \cdot \Delta\bar{\varepsilon} \tag{13}$$

where $\bar{\sigma}_m$, $\Delta\bar{\varepsilon}$, and $\Delta\bar{\sigma}$ are the equivalent components of the mean stress, strain range and stress range. Since studies involving this energy-based approach are yet very limited, no accurate experimental verification of this criterion has been established up to now.

Experimental rig and test procedure

Three different techniques, with different testing systems and specimens, have been used to perform multiaxial fatigue tests: cyclic bending of beams and flat plates, testing of cruciform specimens and thin-walled tubes. The most popular specimen is the thin-walled tube, where deformation can easily be measured by strain gauges or transducers. The state of stress is essentially biaxial, since the stress component through the wall is negligible. The combination of push–pull with cyclic torsion is used more because of its simplicity and the possibility to perform such a test at elevated temperatures. However, it should be noted that the major disadvantage of this combination is the limited range of principal strain ratios ($-\nu \leqslant \varrho \leqslant -1$). On the other hand, a combination of axial load and internal–external pressure allows tests with any circumferential to axial strain ratio. This type of test is complicated, since a pressure vessel is necessary and only a limited amount of work has been done (**26**)(**27**).

In this study, we use this last type of test to perform biaxial low-cycle fatigue tests. Tests were carried out on the modified servo-controlled electro-hydraulic closed-loop MTS system described in (**28**). The loading system allows for an independent simultaneous application of a maximum axial force of 110 kN and a maximum external or internal pressure of 35 MPa. During biaxial fatigue tests, a constant external pressure of 17.5 MPa is applied on the thin-walled tubular specimen through a pressure vessel, while a cyclic internal pressure is introduced inside the specimen. The thin-walled tubes have an external diameter of 27.178 mm, a gauge length of 5.0 mm, and the wall thicknesses are 0.762 mm for negative strain ratios and 0.508 mm for positive strain ratios. A smaller wall thickness was chosen for positive strain ratios to produce sufficiently large plastic strains with the available maximum pressure. They are cut parallel to the rolling direction from a 38.1 mm thick plate, drilled and rough-machined, and subjected to a full anneal in an inert-atmosphere oven at 870°C for one hour. Final machining is performed with progressively fine cuts until the required dimensions are attained. The multistage process followed in designing this specimen is explained in (**29**).

The deformations were measured with a 5 mm gauge length axial extensometer and a diametral extensometer with a flexible semi-circle holding it against the tube at two opposite locations.

The servo-controlled biaxial test machine is used in conjunction with a 48K, 8 simultaneous input channel digital data acquisition system described in (**28**). Measurements from load cells, pressure tensors, LVDTs and transducers are transmitted to the data acquisition system through the servo-controllers. Assembler language programs have been developed in order to allow data acquisition in a real time environment. A program reads and stores all required information in memory; afterwards, BASIC language programs reduce the data and transform them to their physical units before storing them on diskette and displaying them on a terminal or printer.

Table 1 Uniaxial mechanical properties of A-516 Grade 70 steel obtained from solid cylindrical specimens

	Direction	
Properties	*Longitudinal*	*Transverse*
E (MPa)	204 000	205 000
$\sigma_{0.2\%}$ (MPa)	325	358
σ_f (MPa)	993	994
ε_f	0.386	0.396
n'	0.193	0.222
σ'_f (MPa)	841	938
ε'_f	0.204	0.314
c	−0.499	−0.512
b	−0.102	−0.114

The material chosen for this investigation was ASTM A-516 Grade 70 carbon low-alloy steel used in the manufacture of high-temperature pressure vessels. First, uniaxial static and cyclic tests with solid cylindrical specimens have been completed. The chemical composition, the mechanical static properties, the cyclic response, and the uniaxial fatigue curve have been reported in (**22**). Some uniaxial mechanical properties obtained from solid specimens cut parallel (longitudinal direction) and perpendicular (transverse direction) to the plate rolling direction are given in Table 1. These results show that the material has approximately the same mechanical properties in the longitudinal and transverse directions. In a second series of tests, fully-reversed constant-amplitude strain-controlled tests on thin-walled tubular specimens were conducted at room temperature.

The controlled strain ratios ($\varrho = \Delta\varepsilon_t/\Delta\varepsilon_a$) were: −1.25, −1.0, −0.80, uniaxial, 0.0, 0.5, and 1.0, and the fatigue life varied from 180 to 82 000 cycles. The uniaxial strain ratio results of the application of an equal internal–external pressure and a cyclic axial load on the specimen. During each test, maximum and minimum values of axial and circumferential strains and stresses were recorded at each desired number of cycles. The fracture time was determined when the stress amplitude in any direction became unstable which may be considered equivalent to the development of an engineering crack. A 5 per cent variation from the stabilized stress level is generally adopted by workers using thin-walled tubular specimens under pressure (**11**). Depending on the kind of test and the location of crack, the axial or circumferential stress amplitude either decreased or increased.

Fatigue results

The variables measured during biaxial fatigue testing under axial load and pressure are the axial strain amplitude, e_a, the circumferential strain amplitude,

e_t, the axial force, F, the internal pressure, P_i, and the constant external pressure, P_e. The principal true stress ranges are as follows

$$\begin{aligned} \Delta\sigma_a &= (\sigma_a^{max} - \sigma_a^{min})(1 + \varepsilon_a) \\ \Delta\sigma_t &= (\sigma_t^{max} - \sigma_t^{min})(1 + \varepsilon_t) \\ \Delta\sigma_r &\approx 0 \end{aligned} \tag{14}$$

where the superscripts max and min indicate maximum and minimum stresses, respectively. In terms of the measured parameters, we get

$$\begin{aligned} \sigma_a^{max} &= \frac{F^{max} + \Pi d_i^2 P_i^{min}/4}{A_o} \\ \sigma_a^{min} &= \frac{F^{min} + \Pi d_i^2 P_i^{max}/4}{A_o} \end{aligned} \tag{15}$$

for $\varrho \leqslant -\nu$ and

$$\begin{aligned} \sigma_a^{max} &= \frac{F^{max} + \Pi d_i^2 P_i^{max}/4}{A_o} \\ \sigma_a^{min} &= \frac{F^{min} + \Pi d_i^2 P_i^{min}/4}{A_o} \end{aligned} \tag{16}$$

for $\varrho > -\nu$. For all strain ratios, the circumferential stress components are given by

$$\begin{aligned} \sigma_t^{max} &= \frac{d_m}{2t}(P_i^{max} - P_e) \\ \sigma_t^{min} &= \frac{d_m}{2t}(P_i^{min} - P_e) \end{aligned} \tag{17}$$

The experimental stress and strain components computed from measured variables for 44 tests on thin-walled tubes in biaxial low-cycle fatigue, are reported in Table 2. It can be noted that the strain amplitudes are small for the two positive strain ratios of 0.5 and 1.0, since at higher cyclic strain ranges, there is some buckling of the specimen.

The elastic and plastic components of the axial and circumferential strains are given by

$$\begin{aligned} \varepsilon_a^e &= \Delta\sigma_a/2E_a^\varrho, \qquad \varepsilon_a^P = \varepsilon_a - \varepsilon_a^e \\ \varepsilon_t^e &= \Delta\sigma_t/2E_t^\varrho, \qquad \varepsilon_t^P = \varepsilon_t - \varepsilon_t^e \end{aligned} \tag{18}$$

where E_a^ϱ and E_t^ϱ are, respectively, the axial and circumferential elastic moduli, the mathematic expressions of which are

$$E_a^\varrho = \frac{E(1 + \nu^e\varrho)}{1 - (\nu^e)^2}, \qquad E_t^\varrho = \frac{E(1 + \nu^e/\varrho)}{1 - (\nu^e)^2} \tag{19}$$

Table 2 Biaxial fatigue data

Specimen No.	$\varrho = \frac{\varepsilon_t}{\varepsilon_a}$	$\varepsilon_a(\pm)$ (%)	$\varepsilon_t(\pm)$ (%)	σ_a^{max} (*MPa*)	σ_a^{min} (*MPa*)	σ_t^{max} (*MPa*)	σ_t^{min} (*MPa*)	N_f (*cycles*)
K39	1.0	0.078	0.078	227	−115	192	−232	21 000
K05	1.0	0.100	0.100	238	−190	227	−254	3000
K06	1.0	0.125	0.125	265	−189	261	−271	1660
K02	1.0	0.150	0.150	255	−205	285	−291	600
K38	1.0	0.198	0.198	293	−221	309	−318	240
J01	1.0	0.200	0.200	318	−250	296	−303	535
J02	1.0	0.247	0.247	316	−230	333	−350	300
K10	0.50	0.130	0.065	268	−222	178	−212	9500
K12	0.50	0.164	0.082	296	−250	210	−228	2500
K14	0.50	0.196	0.098	320	−228	219	−234	1800
K17	0.50	0.229	0.115	310	−230	259	−274	650
K15	0.50	0.262	0.131	336	−250	268	−277	325
K23	0.0	0.172	0.0	291	−243	72	−110	56 000
K21	0.0	0.217	0.0	310	−248	99	−124	24 000
K18	0.0	0.260	0.0	350	−279	132	−150	11 200
K22	0.0	0.302	0.0	355	−286	126	−138	7400
K36	0.0	0.346	0.0	379	−303	122	−140	3200
K32	0.0	0.432	0.0	388	−323	140	−152	650
K35	0.0	0.514	0.0	433	−341	163	−167	180
H22	uni.	0.200	−0.069	278	−256	0	0	66 000
J10	uni.	0.250	−0.083	309	−291	0	0	37 000
H04	uni.	0.300	−0.105	361	−294	0	0	12 800
J05	uni.	0.350	−0.130	361	−330	0	0	10 700
H02	uni.	0.400	−0.154	404	−335	0	0	4500
J15	uni.	0.500	−0.215	403	−370	0	0	3300
H25	uni.	0.600	−0.240	420	−364	0	0	2000
H26	uni.	0.700	−0.305	446	−387	0	0	700
H20	−0.80	0.189	−0.149	239	−200	113	−130	82 000
J12	−0.80	0.236	−0.186	266	−220	116	−128	39 500
J14	−0.80	0.283	−0.227	275	−215	133	−146	21 500
J04	−0.80	0.330	−0.266	295	−254	110	−134	11 000
H21	−1.0	0.174	−0.174	212	−155	155	−165	38 000
J13	−1.0	0.216	−0.216	232	−172	158	−158	21 000
H09	−1.0	0.260	−0.260	259	−225	61	−260	8000
J03	−1.0	0.303	−0.303	235	−198	175	−195	5700
H06	−1.0	0.340	−0.340	262	−232	73	−281	3100
H05	−1.0	0.430	−0.430	227	−263	83	−304	1900
H32	−1.25	0.151	−0.189	161	−124	186	−210	19 000
J06	−1.25	0.189	−0.234	168	−130	190	−210	9000
H29	−1.25	0.226	−0.282	208	−161	198	−210	5100
J16	−1.25	0.265	−0.330	201	−165	210	−227	2500
H28	−1.25	0.300	−0.375	197	−166	213	−243	1600
H30	−1.25	0.376	−0.467	230	−185	218	−245	1200
H31	−1.25	0.452	−0.564	230	−195	235	−276	560

Table 3 Mechanical cyclic properties of A-516 Grade 70 steel obtained from thin-walled tubular specimens

Direction	ϱ	E^{ϱ} (*MPa*) *Theoretical* (*MPa*)	E^{ϱ} (*MPa*) *Experimental* (*MPa*)	n′	σ'_f (*MPa*)	ε'_f (%)	b	c
Axial	1.00	267 125	251 430	0.112	441	16.9	−0.075	−0.631
	0.50	238 730	214 000	0.133	494	2.9	−0.069	−0.451
	0.00	210 335	203 810	0.162	786	35.0	−0.098	−0.250
	uni.	195 000	195 150	0.234	834	10.9	−0.101	−0.400
	−0.80	164 900	158 870	0.212	692	15.7	−0.101	−0.505
	−1.00	153 545	158 770	0.250	598	11.6	−0.110	−0.475
	−1.25	139 350	139 565	0.245	448	7.5	−0.115	−0.505
Circumferential	1.00	267 125	240 000	0.132	486	21.9	−0.084	−0.509
	0.50	323 915	324 000	0.184	503	1.8	−0.105	−0.410
	0.00	–	–	–	–	–	–	–
	uni.	–	–	–	–	–	–	–
	−0.80	139 350	130 000	0.191	241	8.8	−0.062	−0.529
	−1.00	153 545	138 000	0.201	345	10.4	−0.076	−0.479
	−1.25	164 900	158 775	0.169	402	12.4	−0.075	−0.476

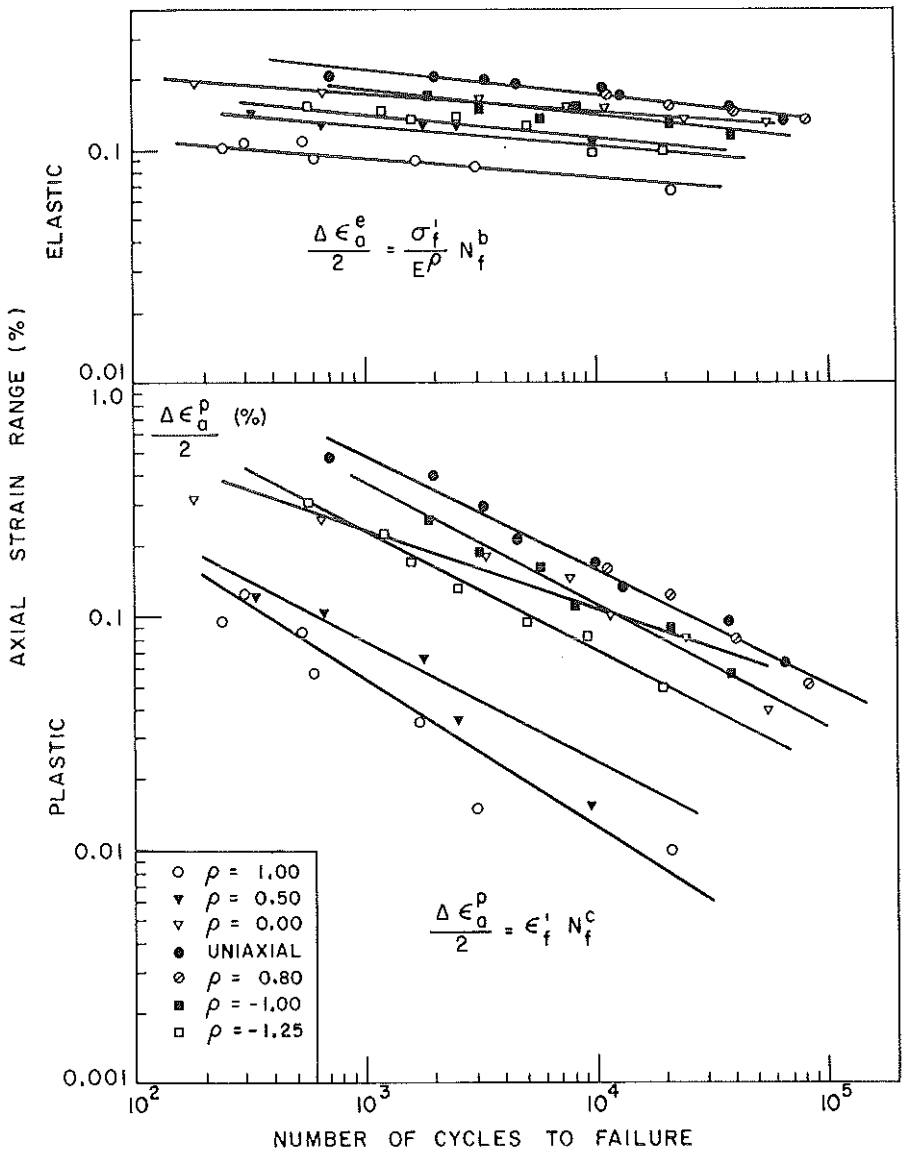

Fig 1 Fatigue curves

The theoretical values of these elastic moduli are reported in Table 3 for each strain ratio and compared with their experimental values obtained graphically from the stable hysteresis loop. A maximum divergence of 10 per cent is observed between the theoretical and the experimental values, due principally to the graphical approximations.

For each strain ratio, the fatigue behaviour may be described by the Coffin–Manson law

$$\frac{\Delta\varepsilon}{2} = \frac{\Delta\varepsilon^{e}}{2} + \frac{\Delta\varepsilon^{P}}{2} = \frac{\sigma'_f}{E^{o}} N_f^{b} + \varepsilon'_f N_f^{c} \tag{20}$$

This relation is represented in Fig. 1 for the experimental data in the axial direction. The coefficients σ'_f and ε'_f and the exponents b and c, determined by the least square technique, are given in Table 3. It can be seen that there is a very small scattering of data around each fatigue curve and that the positive strain ratios are more damaging than the negative strain ratios. Similar observations have been made by Ellison and Andrews (**11**) concerning the high-strain fatigue behaviour of aluminium alloy RR58, tested under identical conditions.

Fatigue life prediction

It has been shown in the historical review that fatigue failure criteria in multiaxial low-cycle fatigue were primarily derived from yield theories and high-cycle fatigue criteria. Because of the unsatisfactory predictions obtained with these criteria, new theories have been proposed, which take into account the factors governing the mechanism of failure. The aim of this study is to examine the hydrostatic stress effect on the fatigue life and to derive stress-based and strain-based criteria which satisfy the following conditions.

(i) They should have a physical interpretation and be based on the mechanism of fatigue crack growth.
(ii) They should take into account the effect of the hydrostatic stress (or strain) and of the change in ductility.
(iii) They should be derived from simple laboratory test data obtained from push–pull and cyclic torsion tests.

Stress-based fatigue failure criterion

Failure criteria for combined cyclic stress can be represented in terms of parametric families of failure surfaces in stress space (**1**)(**5**). For isotropic materials and biaxial state of stress ($\sigma_3 \approx 0$), they are expressed in terms of the cyclic stress invariants by

$$G(I_1, I_2, N_f) = 0 \tag{21}$$

A more specific form, based on Sines' relation (equation (3)) can be expressed as follows

$$a\sqrt{(3J_2)} + bI_1 = \sigma_F \tag{22}$$

where $J_2 = (\frac{1}{3}I_1^2 - I_2)$ is the second deviatoric cyclic stress invariant equivalent to the von Mises effective stress $\bar{\sigma}$, and $\sigma_F = f(N_f)$ is the failure stress at a given fatigue life in the uniaxial case.

Parameters a and b may then be evaluated from experimental results, knowing that for an isotropic material, the sum of a and b has to be equal to one. This condition will be fulfilled and the hydrostatic stress effect and change in ductility will be taken into account by introducing the triaxiality factor $TF = I_1/(3J_2)^{1/2}$ in equation (22). We get

$$\frac{2}{2 + TF}\sqrt{(3J_2)} + \frac{TF}{2 + TF} I_1 = \sigma_F \tag{23}$$

According to this relation, failure occurs at a given fatigue life in biaxial low-cycle fatigue when the modified equivalent stress amplitude σ_s, equal to the left-hand side of equation (23), reaches the value of the uniaxial stress amplitude for failure at the same number of cycles. The modified equivalent stress, σ_s, computed from derived stress components given in Table 3, is plotted for all strain ratios against cycles to failure in Fig. 2. An excellent correlation is obtained for fatigue lives between 10^3 and 10^5 cycles. For very short fatigue lives ($N_f < 800$ cycles), only data at positive strain ratios are available and relation (23) overestimates the fatigue life. For these strain ratios, severe stress conditions on the very thin-walled tubes should lead to strain distortion and buckling which should reduce the fatigue life. In Fig. 3, equation (23) is represented by constant life lines in the stress plane $\{TF/(2 + TF)\}I_1$ vs $\{2/(2 + TF)\}\bar{\sigma}$. Failure lines are drawn from uniaxial fatigue failure data through two points, the coordinates of which are $(0, \sigma_F)$ for pure torsion, and

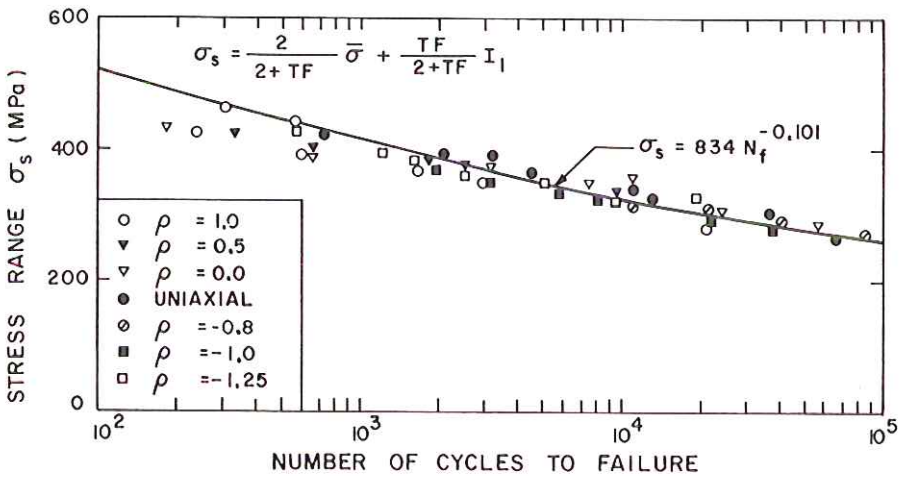

Fig 2 Correlation of biaxial fatigue data by stress parameter σ_s

Table 4 Derived stress and strain components

Specimen No.	$\bar{\sigma}$ *(MPa)*	I_J *(MPa)*	τ_{max} *(MPa)*	ε_a^P (%)	ε_t^P (%)	ε_r^P (%)	ε_r (%)	$\bar{\varepsilon}$ (%)	ε_m (%)	$\gamma_{max}/2$ (%)	ε_n (%)	N_f *(cycles*
K39	195.0	383.0	85.5	0.0100	−0.0104	0.0004	−0.0574	0.0987	0.0985	0.0677	0.0103	21 000
K05	228.5	454.4	107.0	0.0149	−0.0003	−0.0146	−0.0831	0.0314	0.1168	0.0916	0.0084	3000
K06	249.0	493.0	113.5	0.0347	0.0141	−0.0488	−0.1232	0.1772	0.1267	0.1241	0.0009	1660
K02	264.0	518.0	115.0	0.0585	0.0299	−0.0884	−0.1666	0.2241	0.1333	0.1583	−0.0083	600
K38	289.0	570.5	128.5	0.0958	0.0673	−0.1631	−0.2492	0.3140	0.1467	0.2236	−0.0256	240
J01	292.0	583.5	142.0	0.0870	0.0742	−0.1613	−0.2492	0.3173	0.1498	0.2246	−0.0246	535
J02	313.0	614.5	136.5	0.1384	0.1046	−0.2430	−0.3358	0.4100	0.1581	0.2914	−0.0444	300
K10	224.0	440.0	122.5	0.0155	0.0048	−0.0203	−0.0849	0.1384	0.1101	0.1075	0.0225	9500
K12	250.5	492.0	136.5	0.0364	0.0144	−0.0508	−0.1230	0.1835	0.1230	0.1435	0.0205	2500
K14	253.5	500.5	137.0	0.0680	0.0281	−0.0961	−0.1693	0.2340	0.1247	0.1826	0.0134	1800
K17	268.0	536.5	135.0	0.1028	0.0327	−0.1356	−0.2127	0.2813	0.1313	0.2208	0.0082	650
K15	283.0	565.5	146.5	0.1251	0.0469	−0.1720	−0.2537	0.3269	0.1393	0.2579	−0.0234	325
K23	235.0	358.0	133.5	0.0410	0.0000	−0.0410	−0.0894	0.1692	0.0826	0.1307	0.0413	56 000
K21	243.0	390.5	139.5	0.0801	0.0000	−0.0801	−0.1307	0.2221	0.0863	0.1739	0.0431	24 000
K18	273.0	455.5	157.0	0.1057	0.0000	−0.1057	−0.1628	0.2680	0.0972	0.2114	0.0486	11 200
K22	279.0	452.5	160.0	0.1447	0.0000	−0.1447	−0.2029	0.3183	0.0991	0.2525	0.0495	7400
K36	298.0	472.0	170.5	0.1787	0.0000	−0.1787	−0.2406	0.3668	0.1054	0.2933	0.0527	3200
K32	309.5	501.5	178.0	0.2576	0.0000	−0.2576	−0.3221	0.4642	0.1099	0.3770	0.0550	650
K35	336.5	552.0	193.5	0.3241	0.0000	−0.3241	−0.3943	0.5525	0.1197	0.4542	0.0598	180

H22	267.0	267.0	133.5	0.0632	−0.0321	−0.0311	−0.0681	0.1977	0.0629	0.1345	0.0655	66 000
J10	300.0	300.0	150.0	0.0963	−0.0415	0.0548	−0.0963	0.2490	0.0707	0.1731	0.0769	37 000
H04	327.5	327.5	164.0	0.1322	−0.0597	−0.0725	−0.1178	0.2990	0.0772	0.2089	0.0911	12 800
J05	345.5	345.5	173.0	0.1730	−0.0822	−0.0908	−0.1386	0.3513	0.0814	0.2433	0.1057	10 700
H02	369.5	369.5	185.0	0.2107	−0.1029	−0.1078	−0.1589	0.4008	0.0871	0.2795	0.1205	4500
J15	386.5	386.5	193.0	0.3019	−0.1615	−0.1404	−0.1939	0.5062	0.0911	0.3575	0.1425	3300
H25	392.0	392.0	196.0	0.3991	−0.1858	−0.2134	−0.2676	0.6001	0.0924	0.4338	0.1662	2000
H26	416.5	416.5	208.0	0.4866	−0.2474	−0.2392	−0.2968	0.7095	0.0982	0.5025	0.1975	700
H20	299.0	98.0	170.5	0.0508	−0.0555	0.0047	−0.0118	0.2171	0.0282	0.1690	0.0200	82 000
J12	322.0	121.0	182.5	0.0830	−0.0922	0.0091	−0.0128	0.2694	0.0372	0.2110	0.0250	39 500
J14	337.0	105.5	192.0	0.1288	−0.1197	−0.0091	−0.0264	0.3247	0.0296	0.2550	0.0280	21 500
J04	352.0	152.5	198.0	0.1572	−0.1722	0.0149	−0.0143	0.3760	0.0497	0.2980	0.0320	11 000
H21	298.0	23.5	172.0	0.0584	−0.0581	−0.0004	−0.0002	0.2209	−0.0002	0.1740	0.0000	38 000
J13	312.5	44.0	180.0	0.0888	−0.0995	0.0107	0.0060	0.2717	0.0080	0.2150	0.0010	21 000
H09	351.0	81.5	201.0	0.1076	−0.1437	0.0361	0.0228	0.3263	0.0228	0.2600	0.0000	8000
J03	348.0	31.5	201.0	0.1666	−0.1679	0.0013	0.0005	0.3781	0.0015	0.3025	0.0005	5700
H06	369.0	70.0	212.0	0.1844	−0.2117	0.0273	0.0172	0.4230	0.0172	0.3400	0.0000	3100
H05	403.0	76.5	232.0	0.2599	−0.2898	0.0298	0.0188	0.5327	0.0188	0.4300	0.0000	1900
H32	296.0	−55.5	170.0	0.0489	−0.0643	0.0154	0.0238	0.2169	−0.0142	0.1700	−0.0190	19 000
J06	303.5	−51.0	174.5	0.0822	−0.1080	0.0258	0.0329	0.2684	−0.0121	0.2115	−0.0225	9000
H29	336.5	−19.5	194.0	0.0938	−0.1535	0.0597	0.0583	0.3232	0.0023	0.2540	−0.0280	5100
J16	348.0	−35.5	201.0	0.1339	−0.1924	0.0585	0.0609	0.3753	−0.0041	0.2975	−0.0325	2500
H28	355.5	−46.5	205.0	0.1700	−0.2314	0.0614	0.0665	0.4239	−0.0085	0.3375	−0.0375	1600
H30	380.0	−24.0	219.5	0.2273	−0.3212	0.0939	0.0928	0.5992	0.0018	0.4215	−0.0455	1200
H31	406.0	−43.0	234.0	0.2997	−0.4031	0.1033	0.1065	0.6330	−0.0055	0.5080	−0.0560	560

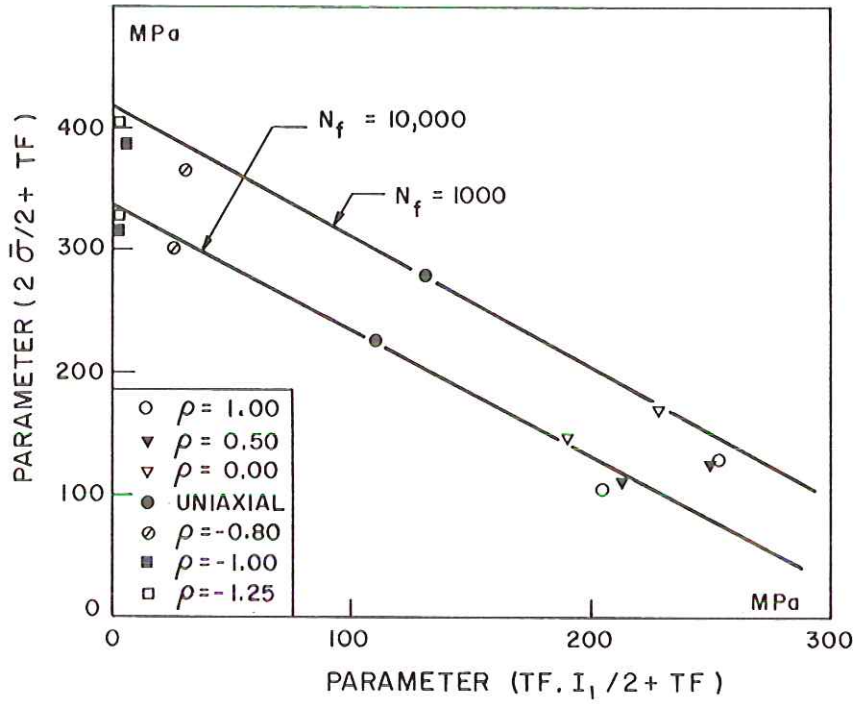

Fig 3 Constant life contours in stress plane

$(0.333\sigma_F, 0.666\sigma_F)$ for uniaxial loading. It can be seen that experimental data derived from results given in Table 4 fall very close to the constant fatigue lines at 10^3 and 10^4 cycles.

Strain-based failure criterion

In multiaxial low-cycle fatigue, failure criteria are most frequently based on strain parameters since strain amplitudes are usually controlled. In biaxial low-cycle fatigue, the state of strain is triaxial and determination of the three principal strains is required. When thin-walled tubes are submitted to combinations of cyclic axial load and pressure, the axial, circumferential, and radial strains are principal strains such as $\varepsilon_1 = \varepsilon_a$, $\varepsilon_2 = \varepsilon_t$, and $\varepsilon_3 = \varepsilon_r$ for $1 \leqslant \varrho \leqslant -\nu$ and $\varepsilon_1 = \varepsilon_a$, $\varepsilon_2 = \varepsilon_r$, and $\varepsilon_t = \varepsilon_3$ for $-\nu \leqslant \varrho \leqslant -1$. The true axial and circumferential strains are given by $\varepsilon_a = \ln(1 + e_a)$, and $\varepsilon_t = \ln(1 + e_t)$ where e_a and e_t are the conventional strains measured and held constant during each test. The true radial strain is given by

$$\varepsilon_r = -\frac{\nu^e}{1 - \nu^e}(\varepsilon_a^e + \varepsilon_t^e) - \frac{\nu^p}{1 - \nu^p}(\varepsilon_a^p + \varepsilon_t^p) \tag{24}$$

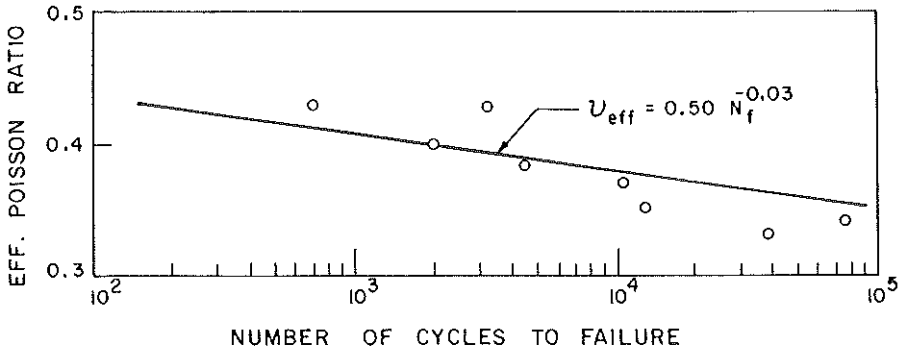

Fig 4 Variation of Poisson's ratio with fatigue life

where the elastic and plastic strain components are determined by equation (18).

In most studies published in the literature, these components are not available, and the third principal strain is obtained from the incompressibility condition ($\varepsilon_1 + \varepsilon_2 + \varepsilon_3 = 0$). However, this hypothesis which assumes fully plastic behaviour and a plastic Poisson ratio of 0.50, is not compatible with cyclic behaviour in low-cycle fatigue. Poisson's ratio is constant at its elastic value $\nu^e = 0.27$ in the elastic regions of the hysteresis loop, and increases until it reaches its plastic value in the plastic regions. Therefore, it is relevant to define an effective Poisson ratio, ν_{eff}, depending on the strain range. Variation of this parameter, defined as the ratio of the measured circumferential and axial strains for uniaxial loading, is plotted versus the fatigue life (proportional to the strain range) in Fig. 4. Experimental values vary from 0.34 at 66 000 cycles to 0.43 at 700 cycles. An extrapolation for any strain range may be obtained with the relation $\nu_{eff} = 0.50 N_f^{-0.03}$ drawn through the experimental data in Fig. 4. When the elastic and plastic components of the measured axial and circumferential strains are not available, the radial strain may be approximated by

$$\varepsilon_r = -\frac{\nu_{eff}}{1 - \nu_{eff}} (\varepsilon_a + \varepsilon_t) \tag{25}$$

Strain parameters most frequently used in failure criteria, e.g., the octahedral shear strain, $\bar{\varepsilon}$, the maximum shear strain $\gamma_{max}/2$, the normal strain, ε_n, and the hydrostatic tension, ε_m, are expressed in terms of principal strains by the following relations

$$\begin{aligned} \bar{\varepsilon} &= \frac{\sqrt{2}}{2(1 + \nu_{eff})} \{(\varepsilon_1 - \varepsilon_2)^2 + (\varepsilon_2 - \varepsilon_3)^2 + (\varepsilon_3 - \varepsilon_1)^2\}^{1/2} \\ \gamma_{max}/2 &= (\varepsilon_1 - \varepsilon_3)/2 \\ \varepsilon_n &= (\varepsilon_1 + \varepsilon_3)/2 \\ \varepsilon_m &= (\varepsilon_1 + \varepsilon_2 + \varepsilon_3) \end{aligned} \tag{26}$$

The octahedral shear strain parameter assumes that the failure mechanism is controlled by the distortion energy, while with the maximum shear strain parameter, it is controlled by slip and decohesion processes. The hydrostatic strain effect which influences dislocation mobility and crack growth rate is taken into account by the normal or hydrostatic strain parameters. Experimental values of each of these parameters, derived from data in biaxial low-cycle fatigue of A516 steel, are given in Table 3 for each test, and in Table 4 for constant fatigue lives of 10^3 and 10^4 cycles. Table 4 shows that the parameters $\bar{\varepsilon}$ and $\gamma_{max}/2$ do not allow a satisfactory correlation between data for a given fatigue life. Positive strain ratios are much more damaging, permissible strains being approximately 40–60 per cent lower than those for negative strain ratios. For a given fatigue life, the ratio of maximum shear strain in torsion to that in tension is approximately equal to 1.1, and the ratio of maximum strain in torsion to that in equibiaxial state of strain is approximately equal to 3. For the same ratios, experimental data of Ellison and Andrews (**11**) on RR58 aluminium alloy lead to 1.30 and 2 respectively. The normal strain, ε_n, vanishes in torsion and has very low values for the strain ratios 1.0 and 0.5; the maximum amplitude occurring for uniaxial loading. The hydrostatic tension, ε_m, is also equal to zero in torsion and increases to its maximum value at $\varrho = 1.0$, when strain ratios vary from -1.0 to 1.0.

Three states of strain may be considered for derivation of a strain-based criterion (i.e., torsional, uniaxial, and equibiaxial states of strain). Visual observations of cracked specimens have shown that cracks are inclined at 45 degrees with respect to the axial direction for specimens tested in torsion, they are always perpendicular to the axial direction in the uniaxial case and they are always parallel to the axial direction in the equibiaxial case. For states of strain corresponding to torsion ($-0.75 \geqslant \varrho \geqslant -1.25$), the intermediate principal strain amplitude, as well as ε_n and ε_m are negligible and the fracture mode is essentially controlled by the maximum shear strain. For a uniaxial state of strain with a maximum strain in tension, the other principal strains are in compression and ε_n is larger than ε_m. Since the crack direction is perpendicular to the axial direction, the intermediate strain has no influence on the crack growth and fracture mode is controlled by the maximum shear strain and the tensile strain across the maximum shear strain plane. In the equibiaxial case, Table 4 shows that, for a given fatigue life, the state of strain is such that $\varepsilon_a = \varepsilon_1, \varepsilon_2 = \varepsilon_t = \varepsilon_1, \varepsilon_3 = \varepsilon_r \simeq -\varepsilon_1, \varepsilon_n \approx 0$, and $\varepsilon_m \approx \varepsilon_1$. Cracks propagate in the axial direction according to the case B propagation mode defined by Brown and Miller (**14**), crack openings being influenced by the intermediate principal strain which acts in tension perpendicular to the crack direction.

A strain-based criterion which should represent each of these failure modes could be expressed as follows

$$\gamma_s = \frac{\gamma_{max}}{2} + k\varepsilon_s = C \tag{27}$$

Table 5 Experimental stress and strain components at constant fatigue life

$\varrho = \frac{\varepsilon_t}{\varepsilon_a}$	N_f (*cycles*)	TF	$\bar{\sigma}$ (*MPa*)	I_1 (*MPa*)	σ_S (*MPa*)	ε_a (%)	ε_t (%)	ε_r (%)	$\bar{\varepsilon}$ (%)	$\gamma_{max}/2$ (%)	ε_n (%)	ε_m (%)	γ_S (%)
1.0	1000	1.973	260	513	384	0.155	0.155	−0.170	0.230	0.162	−0.008	0.140	0.438
0.50	1000	1.992	256	510	382	0.206	0.103	−0.180	0.240	0.193	0.001	0.129	0.449
0.0	1000	1.640	308	505	396	0.400	0.000	−0.270	0.420	0.335	0.065	0.130	0.501
uni.	1000	1.000	418	418	418	0.640	−0.260	−0.260	0.640	0.450	0.190	0.120	0.450
−0.80	1000	0.422	438	185	394	0.620	−0.496	−0.022	0.660	0.558	0.062	0.102	0.440
−1.0	1000	0.200	422	85	392	0.480	−0.480	−0.020	0.620	0.480	0.000	−0.020	0.512
−1.25	1000	−0.100	376	−38	398	0.375	−0.469	0.085	0.520	0.422	−0.047	−0.009	0.442
1.0	10 000	1.960	209	410	309	0.086	0.086	−0.069	0.115	0.078	0.009	0.103	0.276
0.50	10 000	1.960	218	428	322	0.138	0.069	−0.085	0.138	0.111	0.027	0.122	0.345
0.0	10 000	1.610	266	428	338	0.251	0.000	−0.150	0.260	0.200	0.050	0.101	0.323
uni.	10 000	1.000	330	330	330	0.330	−0.125	−0.125	0.330	0.228	0.103	0.080	0.228
−0.80	10 000	0.392	354	139	319	0.330	−0.264	−0.016	0.370	0.297	0.033	0.050	0.236
−1.0	10 000	0.147	339	50	319	0.255	−0.255	−0.012	0.320	0.255	0.000	0.012	0.275
−1.25	10 000	−0.135	303	−41	328	0.176	−0.220	0.032	0.260	0.198	−0.022	−0.012	0.225

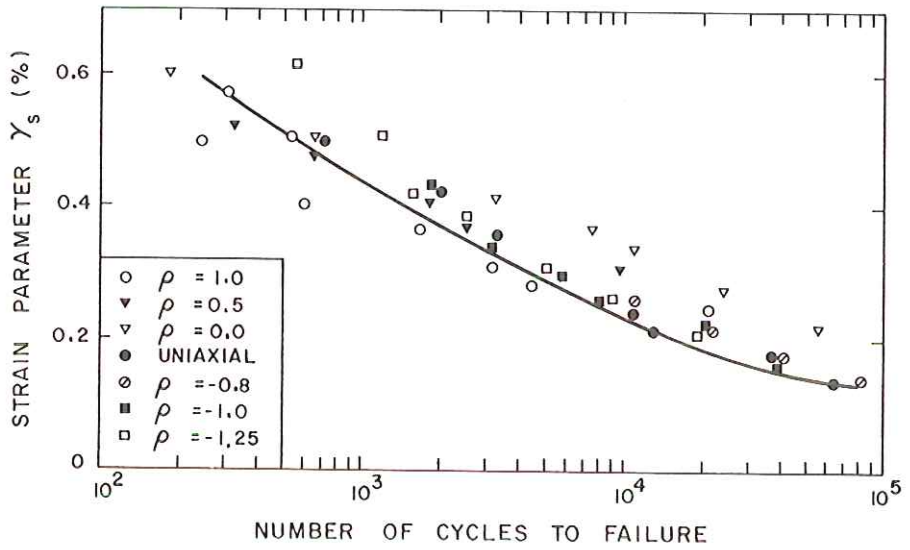

Fig 5 Correlation of biaxial fatigue data by strain parameter γ_s

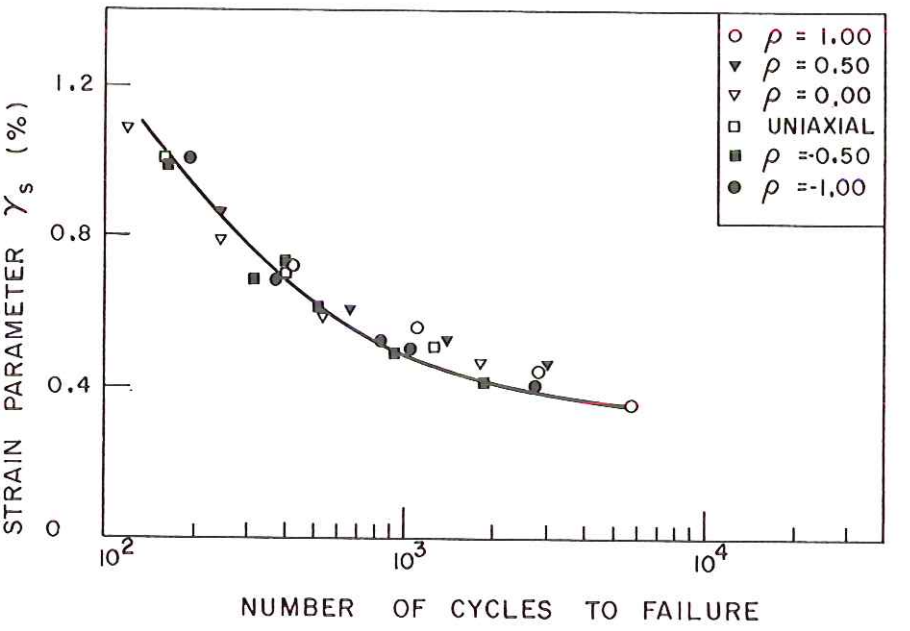

Fig 6 Correlation of biaxial data of Ellison and Andrews (11) by strain parameter γ_s

where $\varepsilon_s = \varepsilon_n$ if $\varrho \leqslant -\nu$ and $\varepsilon_s = \varepsilon_m$ if $\varrho > -\nu$, and k is a parameter depending on the material properties and the state of strain.

For the experimental data obtained on A516 steel, the following specific form is suggested

$$\gamma_s = \frac{\gamma_{max}}{2} + 2\left(TF - \frac{\gamma_{Funi}}{\gamma_{Ftorsion}}\right)\varepsilon_s = C \tag{28}$$

in which γ_{Funi} and $\gamma_{Ftorsion}$ are the maximum shear strain for a given fatigue life for uniaxial and torsional states of strain, respectively.

Equation (28) is plotted in Fig. 5 against cycles to failure. A reasonable correlation is obtained for fatigue lives between 10^3 and 10^5 cycles, except for $\varrho = 0.0$, for which fatigue life is underestimated. For shorter fatigue life, accuracy of data is not sufficient to conclude on the validity of the proposed criterion. As previously mentioned, secondary effects, such as bending strains and buckling, should reduce the fatigue life for positive ratios.

Equation (27) is used for correlating biaxial experimental data of Ellison and Andrews (**11**). When $k = 1$, we obtain an excellent correlation for any fatigue life and any strain ratios, as shown in Fig. 6. For uniaxial and torsional loadings, the strain parameter $\gamma_s = \frac{1}{2}\gamma_{max} + \varepsilon_s$ is identical to the maximum strain, ε_1, while for positive strain ratios, the intermediate principal strain effect on the fatigue life is taken into account by the hydrostatic strain component, ε_m.

Discussion

Attempts have been made to correlate the experimental data on A516 steel with other known failure criteria. Evidence given in Table 4 indicates that stress-based criteria in which the hydrostatic stress effect is not included, i.e., the von Mises and the Tresca criteria, lead to poor correlation. Likewise, criteria based on a combination of maximum shear stress and the normal stress on the maximum shear stress plane underestimate the permissible stress at a given fatigue life for positive strain ratios. Since τ_{max} and σ_n are equal to $\sigma_1/2$ for positive strain ratios, the effect of the intermediate principal stress, which acts in tension perpendicular to the crack direction and influences dislocation mobility, is never considered.

For a chosen strain parameter (equivalent strain, for example), it is generally possible to find empirical expressions for the coefficient C and the exponent α of the Coffin–Manson equation (7) to obtain reasonable correlations with experimental data. Nevertheless, such a relation cannot be used in practice for fatigue life prediction in multiaxial low-cycle fatigue since an extended experimental programme is needed for the determination of C and α, which depend on the strain ratio and the material properties.

Agreement is better when criteria are based on total strain components instead of those based on plastic strain components for the two following reasons: (a) computation of plastic strain range depends on the stress amplitudes and the Young moduli measurement ($\varepsilon^P = \varepsilon^t - \sigma/E$), (b) plastic

strain ranges are negligible for $\varrho = 0.50$ and 1.0 when fatigue lives are greater than 3000 cycles.

This study, as well as other recent works, has shown that the hydrostatic tension effect must be incorporated in multiaxial low-cycle fatigue criteria. Up to now, development of such criteria has been delayed by the limited amount of available data reported in the literature. In future research in multiaxial low-cycle fatigue, an important effort should be made to supply this lack of information. As previously shown, experimental data should include accurate computation of the elastic, plastic, and total components of the three principal strains for strain ratios varying from -1.0 to 1.0. Such experimental research should also be extended to include the effects of temperature, environment, mean stress and out of phase stress.

Conclusion

In this study, experimental data obtained from 44 strain-controlled tests have been presented for biaxial low-cycle fatigue of A516 steel. Tests were performed on thin-walled tubes submitted to combinations of cyclic axial load and fluctuating external–internal pressure at seven strain ratios varying from -1.25 to 1.0. Experimental and derived stress and strain components required for the development or the verification of failure criteria were computed and reported for each test. They have clearly shown that superimposed hydrostatic tension reduces the fatigue life. Two criteria, accounting for the hydrostatic stress or strain effect have been proposed. Each of them is a modification of a yielding theory (von Mises or Tresca) by means of a stress or strain parameter which represents the intermediate principal stress or strain effect on fatigue life.

Acknowledgement

This research was supported by the National Sciences and Engineering Research Council of Canada (NSERC Grant No. A-1001) and le Fonds FCAR du Québec (Grant No. EQ-335). The author would like to thank Laurent Thibodeau, Chief Technician, for helping in carrying out the experiments.

References

(1) KREMPL, E. (1974) The influence of state of stress on low-cycle fatigue of structural materials, *ASTM STP 549*, ASTM, Philadelphia, PA, pp. 1–46.
(2) BROWN, M. W. and MILLER, K. J. (1982) Two decades of progress in the assessment of multiaxial low-cycle fatigue life, *ASTM STP 770*, ASTM, Philadelphia, PA, pp. 482–499.
(3) GARUD, Y. S. (1981) Multiaxial fatigue: a survey of the state-of-the art, *J. Testing Evaluation*, **9**, 165–178.
(4) HASHIN, Z. (1981) Fatigue failure criteria for combined cyclic stress, *Int. J. Fracture*, **17**, 101–109.
(5) SINES, G. (1981) Fatigue criteria under combined stresses or strains, *J. Engng Mater. Technol.*, **103**, 82–90.
(6) McDIARMID, D. L. (1972) *Fatigue criteria and cumulative damage in fatigue under multiaxial stress conditions*, PhD thesis, The City University, London, UK.

(7) ELLYIN, F., LEFEBVRE, D., and NEALE, K. W. (1980) High-strain biaxial fatigue of 2024-T351 aluminum under combined axial stress and torsion, *Advances in Materials Technology in the Americas*, ASME, pp. 17–21.
(8) MATAKE, T. (1977) An explanation on fatigue limit under combined stress, *Bull. Jap. Soc. mech. Engrs*, **20**, 257–263.
(9) FINDLEY, W. N. (1959) A theory for the effect of mean stress on fatigue of metals under combined torsion and axial load or bending, *J. Engng Ind.*, **81**, 301–306.
(10) SHEWCHUK, J., ZAMRIK, S. Y., and MARIN, J. (1968) Low-cycle fatigue of 7075-T651 aluminium alloy in biaxial bending, *Expl Mech.*, 504–512.
(11) ELLISON, E. G. and ANDREWS, J. M. H. (1973) Biaxial cyclic high-strain fatigue of aluminium alloy RR58, *J. Strain Analysis*, **8**, 209–219.
(12) LIBERTINY, G. Z. (1967) Short life fatigue under combined stress, *J. Strain Analysis*, **2**, 91–95.
(13) PASCOE, K. J. and DE VILLIERS, J. W. R. (1967) Low-cycle fatigue of steels under biaxial straining, *J. Strain Analysis*, **2**, 117–126.
(14) BROWN, M. W. and MILLER, K. J. (1973) A theory for fatigue failure under multiaxial stress–strain conditions, *Proc. Instn mech. Engrs*, **187**, 745–755 and D229–D244.
(15) BROWN, M. W. and MILLER, K. J. (1979) High temperature low-cycle biaxial fatigue of two steels, *Fatigue Engng Mater. Structures*, **1**, 217–229.
(16) BLASS, J. J. and ZAMRIK, S. Y. (1979) Multiaxial low-cycle fatigue of Type 304 stainless steel, *1976 American Society of Mechanical Engineers Metal Properties Council Symposium on Creep Fatigue Interaction*, ASME, pp. 129–159.
(17) DAVIS, E. A. and CONNELLY, F. M. (1959) Stress distribution and plastic deformation in rotating cylinders of strain-hardening materials, *J. Appl. Mech.*, 25–30.
(18) MANSON, S. S. and HALFORD, G. R. (1977) Multiaxial low-cycle fatigue of Type 304 stainless steel, *J. Engng Mater. Technol.*, 283–285.
(19) MARLOFF, R. H. and JOHNSON, R. L. (1980) The influence of multiaxial stress on low-cycle fatigue of Cr–Mo–V steel at 1000°F, *Welding Research Council Bulletin*, No. 264, 1–21.
(20) MOWBRAY, D. F. (1980) A hydrostatic stress sensitive relationship for fatigue under multiaxial stress conditions, *J. Testing Evaluation*, **8**, 3–8.
(21) HALFORD, G. R. (1966) The energy required for fatigue, *J. Mater., ASTM*, **1**, 3–18.
(22) LEFEBVRE, D. and ELLYIN, F. (1984) Cyclic response and inelastic strain energy in low-cycle fatigue, *Int. J. Fatigue*, **6**, 9–15.
(23) ELLYIN, F. and KUJAWSKI, D. (1984) Plastic strain energy in fatigue failure, *Trans Am. Soc. Mech. Engrs*, **106**, 342–347.
(24) ELLYIN, F. (1974) A criterion for fatigue under multiaxial states of stress, *Mechanics Res. Comm.*, **1**, 219–224.
(25) LEIS, B. N. (1977) An energy-based fatigue and creep–fatigue damage parameter, *J. Pressure Vessel Technol.*, 524–533.
(26) HAVARD, D. G. (1970) *Fatigue and deformation of normalized mild steel subjected to biaxial cyclic straining*, PhD thesis, University of Waterloo, Canada.
(27) ANDREWS, J. M. H. and ELLISON, E. G. (1973) A testing rig for cycling at high biaxial strains, *J. Strain Analysis*, **8**, 168–175.
(28) LEFEBVRE, D., CHEBL, C., THIBODEAU, L., and KHAZZARI, E. (1983) A high-strain biaxial testing rig for thin-walled tubes under axial load and pressure, *Expl Mech.*, 384–391.
(29) ELLYIN, F. and VALAIRE, B. (1982). High-strain biaxial fatigue test facility, *Proceedings of the 1982 Joint Conference on Experimental Mechanics*, SESA-JSME, Hawaii, pp. 136–143.